Physics of Plasmas LETTERS scitation.org/journal/php

Nonlinear saturation of kinetic ballooning modes by zonal fields in toroidal plasmas

Cite as: Phys. Plasmas **26**, 010701 (2019); doi: 10.1063/1.5066583
Submitted: 15 October 2018 · Accepted: 07 January 2019 · Published Online: 23 January 2019

G. Dong,[1] J. Bao,[2] A. Bhattacharjee,[1] and Z. Lin[2]

AFFILIATIONS

[1] Princeton Plasma Physics Laboratory, Princeton University, Princeton, New Jersey 08540, USA
[2] Department of Physics and Astronomy, University of California, Irvine, California 92697, USA

ABSTRACT

Kinetic ballooning modes (KBMs) are widely believed to play a critical role in disruptive dynamics as well as turbulent transport in magnetic fusion and space plasmas. While the nonlinear evolution of the ballooning modes has been proposed as a mechanism for "detonation" in various scenarios such as the edge localized modes in tokamaks, the role of the kinetic effects in such nonlinear dynamics remains largely unexplored. In this work, global gyrokinetic simulation results of KBM nonlinear behavior are presented. Instead of the finite-time singularity predicted by ideal magnetohydrodynamic theory, the kinetic instability is shown to develop into an intermediate nonlinear regime of exponential growth, followed by a nonlinear saturation regulated by spontaneously generated zonal fields. In the intermediate nonlinear regime, rapid growth of localized current sheets, which can induce magnetic reconnection, is observed.

Ballooning instability (or its astrophysical counterpart, the Parker instability) in a magnetized plasma is driven by local unfavorable magnetic curvature and a pressure gradient.[1] The nonlinear evolution of the instability has been a subject of great interest for a diverse range of eruptive phenomena such as substorms in the Earth's magnetotail[2,3] and edge-localized modes (ELMs)[4] in toroidal fusion plasmas.[5,6] Theoretical studies of nonlinear ideal magnetohydrodynamic (MHD) ballooning modes predict explosive nonlinear growth.[7] Finger-like structures develop, forming a front with a steep pressure gradient which can nonlinearly destabilize the mode, and result in a finite-time singularity ("detonation").[8] However, attempts at simulating such an instability using the full MHD equations have not succeeded in realizing a finite-time singularity. While finger-like structures are indeed observed,[9] the mode is seen to grow in the nonlinear regime exponentially with its linear growth rate. A new asymptotic regime, called the "intermediate" nonlinear regime of exponential growth, has been formulated analytically to account for these simulations.[10] During the intermediate regime, the mode structure becomes sufficiently narrow that the validity of the MHD model is questionable. In collisionless plasmas, kinetic effects intervene. This leads to considerations of the kinetic ballooning mode (KBM) which is recognized to play an important role in the stability and transport of fusion plasmas near the plasma edge,[11,12] as well as substorm dynamics in the Earth's magnetotail.[13,14] However, the nonlinear dynamics of the KBM in toroidal plasmas is not well understood. Flux-tube gyrokinetic simulations of the KBM arrived at contradictory conclusions: zonal flows play a dominant role in KBM saturation in GENE simulations[15] but not in GKV simulations where the zonal flows are seen to be much weaker than that in the ion-temperature-gradient (ITG) turbulence.[16,17] KBM saturation requires external flow shear in GYRO simulations[18] beyond a critical beta value. In BOUT++ gyrofluid simulations,[19] KBM saturates via profile relaxation.

Here, we demonstrate from a global gyrokinetic particle-in-cell simulation that after a linear regime, the KBM evolves into an intermediate regime, followed by a saturated nonlinear regime. In addition to features that are similar to its ideal MHD counterpart,[9] the kinetic intermediate regime also exhibits qualitatively different features. The most important one is that the kinetic electromagnetic dynamics leads to the spontaneous generation of zonal flow (flux-surface-averaged electrostatic potential $\langle\delta\phi\rangle$) and zonal current (flux-surface-averaged vector potential $\langle\delta A_{\parallel}\rangle$). When the zonal flow shear exceeds the linear growth rate, zonal flow shearing suppresses the nonlinear instability which in turn self-regulates the zonal fields (the zonal flow and the zonal current), leading to a saturated nonlinear regime. In the kinetic intermediate regime, thin current sheets develop near the mode rational surfaces, which can eventually exhibit

tearing instability, but the resistive tearing mode growth rate appears to be too slow to have a strong effect on KBM nonlinear saturation.

Gyrokinetic simulation of KBM.—In the simulations using the gyrokinetic toroidal code (GTC),[20] ions are treated by the gyrokinetic Vlasov equation, while electrons are described using the nonlinear fluid equations: the electron perturbed density δn_e is calculated by time-advancing the continuity equation[21] including the diamagnetic (pressure gradient) term which provides the interchange drive, and the electron parallel flow $\delta u_{\|e}$ is calculated by inverting the parallel Ampere's Law.[22] The gyrokinetic Poisson's equation is solved to obtain the perturbed electrostatic potential $\delta\phi$. For the completeness of the model, the parallel magnetic perturbation $\delta B_\|$[23] and the equilibrium current density,[21] which provide an additional linear drive, are kept in the simulation. The parallel vector potential $\delta A_\| = \delta A_\|^{adi} + \delta A_\|^{na}$ is solved for the adiabatic and non-adiabatic parts. Integrating the electron drift kinetic equation to the momentum order, we can derive the linear Ohm's law for adiabatic $\delta A_\|^{adi}$ and the nonlinear Ohm's law[24] for non-adiabatic $\delta A_\|^{na}$ as follows:

$$\frac{\partial \delta A_\|^{adi}}{\partial t} = \frac{c}{B_0}\mathbf{B_0}\cdot\nabla\delta\phi_{ind} \tag{1}$$

and

$$\frac{1}{c}\frac{\partial \delta A_\|^{na}}{\partial t} = \frac{\boldsymbol{\delta B}_\perp}{B_0}\cdot\nabla\delta\phi_{ind} - \frac{m_e}{n_0 e^2}\nabla\cdot\left(\delta u_{\|e}\frac{cP_{e0}\mathbf{B_0}\times\nabla\delta B_\|}{B_0^3}\right) + \frac{P_{e0}}{en_0}\frac{\boldsymbol{\delta B}_\perp}{B_0^2}\cdot\nabla\delta B_\|, \tag{2}$$

where $\mathbf{B_0}$ is the equilibrium magnetic field and $\delta\mathbf{B}_\perp$ is the perturbed perpendicular magnetic field. Here, $\delta\phi_{ind} = \frac{T_e}{e}\left(\frac{\delta n_e}{n_0} - \frac{\delta\psi^{adi}}{n_0}\frac{\partial n_0}{\partial\psi_0}\right) - \delta\phi$ is the inductive potential, $\delta\psi^{adi}$ is the adiabatic component of the perturbed poloidal flux, defined as $\nabla\delta\psi^{adi}\times\nabla\alpha = \nabla\delta A_\|^{adi}\times\mathbf{B_0}/B_0$, $\alpha = q(\psi_0)\theta - \zeta$ is the field-line label with the Boozer poloidal angle θ and toroidal angle ζ, and the safety factor $q(\psi_0)$ is a function of the equilibrium poloidal flux ψ_0. Also, T_e is the electron equilibrium temperature, n_0 is the plasma equilibrium density, and $P_{e0} = n_0T_e$ is the electron equilibrium pressure. The first term on the right-hand-side of Eq. (2) represents the so-called nonlinear ponderomotive force[25] in the fluid electron momentum equation. The nonlinear drive from finite $\delta B_\|$ is obtained in the second and third terms, which are small compared with the nonlinear ponderomotive drive due to the smallness of β. A complete form of the generalized Ohm's law is presented in Ref. 24. In future work, if we consider collisionless micro-tearing mode dynamics or cases with large flow at the plasma edge,[26] the terms associated with electron inertia in the generalized Ohm's law need to be kept. The flux-surface-averaged component of the Poisson's equation and Eq. (2) are solved for the zonal flow and the zonal current, respectively.

In the simulations, Cyclone Base Case parameters are used for the background plasmas: the major radius is $R_0 = 83.5\,cm$, the inverse aspect ratio is $a/R_0 = 0.357$. At $r = 0.5a$, the plasma parameters are $B_0 = 2.01\,T$, $T_e = 2223\,eV$, $R_0/L_T = 6.9$, $R_0/L_n = 2.2$, and $q = 1.4$. The first order s–α model[21] is used for the equilibrium magnetic field. With these parameters and $\beta_e = 2\%$, the KBM is linearly unstable.[23,27] In the linear simulations for a single $n = 10$ toroidal mode, the mode exhibits ballooning mode characteristics, with real frequency $\omega_r^{lin} = 0.77c_s/a$ and growth rate $\gamma^{lin} = 0.63c_s/a$. In the nonlinear simulations, we simulate $n = 10$ toroidal mode (keeping all the poloidal harmonics m), and its nonlinear interaction with the zonal mode ($m = 0$, $n = 0$). The GTC global field-aligned mesh has 32, 400, and 200 grids in the parallel, poloidal, and radial direction, respectively. Convergence studies show that the physical results in the linear and nonlinear simulations are not sensitive to the grid size, time step size, or number of particles per cell.

Intermediate regime and saturation by zonal fields.—A time history for the nonlinear KBM simulation is shown in Fig. 1. The perturbed electrostatic potential, parallel vector potential, and parallel magnetic field are normalized as $e\delta\phi/T_e$, $c\delta A_\|/v_A B_0 R_0$, and $\delta B_\|/B_0$, respectively, where $v_A = B_0/\sqrt{4\pi n_0 m_i}$. The perturbed electrostatic potential $\delta\phi_{10,14}$, the parallel vector potential $\delta A_{\|10,14}$, and the parallel magnetic field $\delta B_{\|10,14}$ of the dominant (10, 14) mode are measured at the mode rational surface with $q = 1.4$ at the center of the simulation domain. The zonal flow $\langle\delta\phi\rangle$ and the zonal current $\langle\delta A_\|\rangle$ amplitude are averaged over the simulation domain. Before $t \sim 11a/c_s$, $\delta\phi_{10,14}$ is seen to grow more than two orders of magnitudes at the linear growth rate γ^{lin} after a brief transient stage. $\delta A_{\|10,14}$ remains much lower than $\delta\phi_{10,14}$, as shown by the diamond solid red line in Fig. 1, since the linear adiabatic component $\delta A_{\|10,14}^{adi}$ is zero at the rational surface, as constrained by Eq. (1). A linear phase shift between $\delta A_{\|10,14}$ and $\delta\phi_{10,14}$ (measured at $q = 1.36$) is about

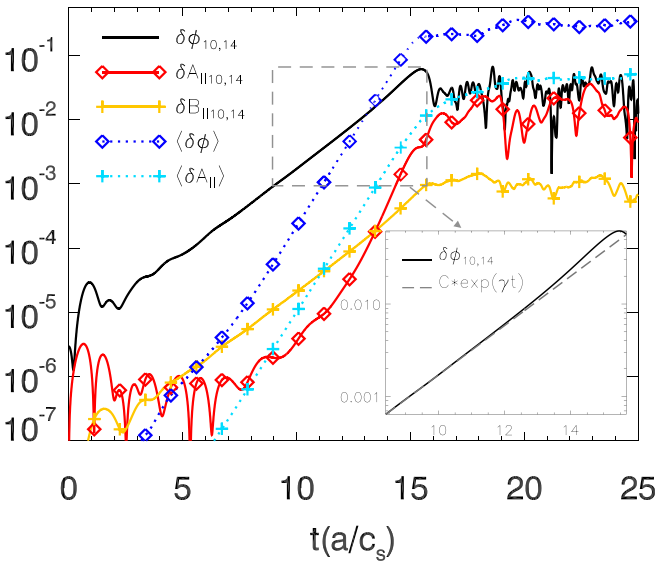

FIG. 1. Time history of the normalized perturbed electrostatic potential $\delta\phi$, parallel vector potential $\delta A_\|$, parallel magnetic field $\delta B_\|$ for the mode ($m = 14$, $n = 10$) measured at the (14, 10) rational surface, and radial averaged zonal flow and zonal current amplitude. Comparison of a linear growth at $\gamma = \gamma^{lin}$ (grey dashed line) and the $\delta\phi$ evolution (black solid line) in the intermediate regime is shown in the zoom-in plot.

0.8π. $\delta B_\parallel$ is much smaller than $\delta\phi$ due to small plasma β. At $t \sim 11a/c_s$, $\delta A_{\parallel 10,14}$ starts to grow faster than exponential, indicating that the mode evolves into a nonlinear regime where ponderomotive effects become important. From $t \sim 11a/c_s$ to $t \sim 15a/c_s$, $\delta\phi_{10,14}$ and $\delta B_{\parallel 10,14}$ grow slightly faster than exponential, with an effective growth rate $\gamma^{int} = 1.1\gamma^{lin}$. A comparison of $\delta\phi_{10,14}$ evolution with a pure linear growth is shown in the zoom-in plot in Fig. 1. During this regime, the field quantities retain their linear poloidal mode structure. These features are qualitatively similar to those in the intermediate regime found in compressible MHD simulations.[9] The growth of dominant field quantities at a rate faster than the linear growth rate indicates that the perfect cancellation between nonlinear destabilization due to enhanced pressure gradients and stabilization due to field-line bending that occurs in the ideal MHD dynamics[10] does not occur in this kinetic intermediate regime. We characterize the intermediate regime of the KBM by the rapid growth of the tearing component of $\delta A_\parallel$ at the rational surface (starting around $t = 11a/c_s$ in this case), and the close-to-exponential growth of $\delta\phi$ and $\delta B_\parallel$. Mode saturation (at around $t = 15a/c_s$ in this case) indicates the end of the intermediate regime. In the linear regime and the intermediate regime, $\langle\delta\phi\rangle$ and $\langle\delta A_\parallel\rangle$ both grow exponentially at a growth rate $\gamma^{zonal} \sim 2\gamma^{lin}$. This suggests that the zonal fields in KBM are passively generated by three-wave coupling, in contrast to the zonal flow excitation by modulational instabilities in electrostatic ITG, where $\langle\delta\phi\rangle$ grows as a double exponential function.[28]

At $t \sim 15a/c_s$, the dominant mode and the zonal fields saturate nonlinearly. As shown by the diamond dotted blue line in Fig. 1, the steady state zonal flow amplitude is around 5 times larger than the dominant $\delta\phi_{10,14}$ component. The ion energy transport reaches steady state at the gyro-Bohm level with $\chi_i \sim \chi_{GB}$, as shown by the black solid line in Fig. 2, where $\chi_{GB} = \rho_i^2 v_i/a$, $v_i = \sqrt{T_i/m_i}$, and $\rho_i = v_i m_i c/eB_0$. The ion heat conductivity $\chi_i = \frac{1}{n_0 \nabla T_i}\int d\mathbf{v}(\frac{1}{2}m_i v^2 - \frac{3}{2}T_i)v_r \delta f$ is defined as the volume averaged ion energy flux normalized by the local temperature gradient, where v_r is the radial drift velocity including the $E \times B$ drift and the magnetic flutter drift.[24] In the simulation

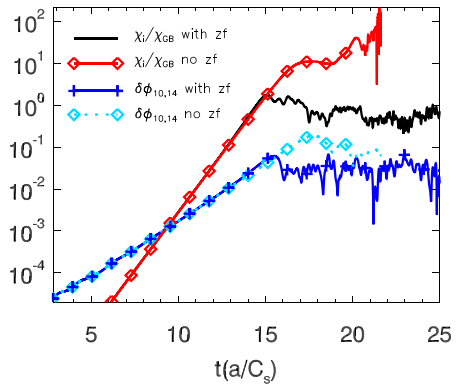

FIG. 2. Time history is shown for the ion heat conductivity χ_i and the perturbed electrostatic potential $\delta\phi$ for the mode ($m = 14$, $n = 10$) in a simulation with self-consistently generated zonal flow and zonal current and in a simulation with artificially suppressed zonal fields.

where the zonal flow and the zonal current are both artificially suppressed, the nonlinear ion heat conductivity becomes one order of magnitude larger, as shown by the diamond red line in Fig. 2. $\delta\phi_{10,14}$ also saturates at a magnitude around 3 times higher than that in the case with the zonal fields. In two other simulations where only the zonal current or the zonal flow is artificially suppressed, $\delta\phi$ and χ_i saturation levels also see a significant increase, indicating that both zonal flow and zonal current regulate ion energy transport and KBM saturation. A comparison of the $\delta\phi$ nonlinear poloidal structure between simulations with and without the zonal fields is shown in Fig. 3. In the simulation with self-consistently generated zonal flow and zonal current, the zonal fields break up the radially elongated eigenmode structure into microscale and mesoscale structures as in Fig. 3(a), reducing radial transport. The radial variation scale length of the zonal fields is on the order of the distance between the rational surfaces. In the simulation with the zonal fields artificially suppressed, although the non-zonal nonlinear $E \times B$ term also shears the mode structure, some macroscale radial filaments of streamers survive. These results show that the KBM saturation is governed by the zonal fields, including both the zonal flow and the zonal current. In two additional simulations where $\beta_e = 1.74\%$ and $\beta_e = 1.55\%$ (near the KBM instability threshold), we observe similar nonlinear saturation features. In simulations with $\beta_e = 2\%$, but without $\delta B_\parallel$ and equilibrium current, we also observe similar nonlinear KBM dynamics.

Onset of nonlinear rapid growth of the localized current sheet.—As shown by the diamond solid red line in Fig. 1, $\delta A_{\parallel 10,14}$ at the mode rational surface first grows faster than exponential and then grows more than one order of magnitude exponentially with a nonlinear growth rate $\gamma^{nl} \sim 3\gamma^{lin}$ during the intermediate regime. This growth rate can be explained by the coupling between the zonal current and non-zonal inductive potential through the first term in Eq. (2). The poloidal $\delta A_\parallel$ structure evolves from the linear eigenmode structure at $t = 11c_s/a$, as shown in Fig. 4(a), to mesoscale structures at $t = 17c_s/a$, as shown in Fig. 4(b). The mode structure becomes thin in the radial direction. This corresponds to the rapid growth of current sheets localized at the rational surfaces, excited by the nonlinear ponderomotive force terms in Eq. (2). In the simulation where the nonlinear ponderomotive force terms are not included ($\delta A_\parallel^{na} = 0$), although zonal flows still break the linear mode into mesoscale structures nearly isotropic in radial and poloidal directions, as shown in Fig. 4(c), the radial correlation length of the turbulence eddies is much longer than that in the case with the self-consistent ponderomotive force.

The development of the localized current sheet in the intermediate and nonlinear regime in KBM is analogous to the nonlinear process in the ideal MHD theory. However, in this scenario where the kinetic effects become important during the intermediate regime, the mode saturates at the spatial scale comparable to the ion gyroradius with a transport level controlled by the zonal fields. In contrast, the mode structure in the MHD theory tends to become singular until the pressure profile flattens by transport. The radial profiles of (n,m) harmonic of $\delta A_\parallel$ at $t = 11c_s/a$ and $t = 17c_s/a$ are shown in Figs. 4(d) and 4(e). The linear mode structure has exact odd parity at the rational

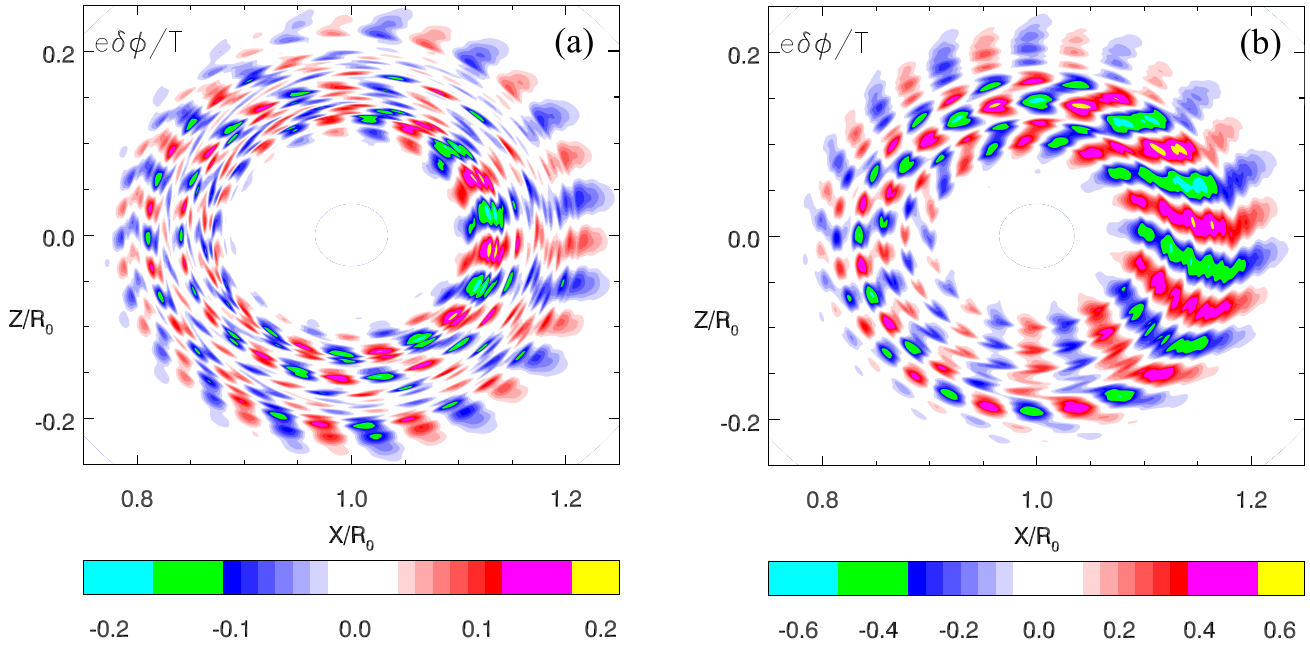

FIG. 3. Poloidal contour of the perturbed electrostatic potential $\delta\phi$ at the nonlinear regime. Panel (a) shows broken radial filaments in the simulation with self-consistently generated zonal flow and zonal current. Panel (b) shows macroscale radial filaments in the simulation with the zonal fields artificially suppressed. To clearly illustrate the difference in radial filaments, the $\langle\delta\phi\rangle$ component is not plotted in (a).

surfaces, and the nonlinear mode structure contains even parity component at the rational surfaces driven by the nonlinear electromagnetic ponderomotive force. For comparison, Fig. 4(f) shows the (n,m) harmonic of $\delta A_{\parallel}$ after saturation in the simulation with $\delta A_{\parallel}^{na} = 0$. In this case, each (n,m) harmonic is still zero at the $q = m/n$ surface. Because of the formation of a thin current layer near rational surfaces, we conducted simulations with finite resistivity in the generalized Ohm's law to test the

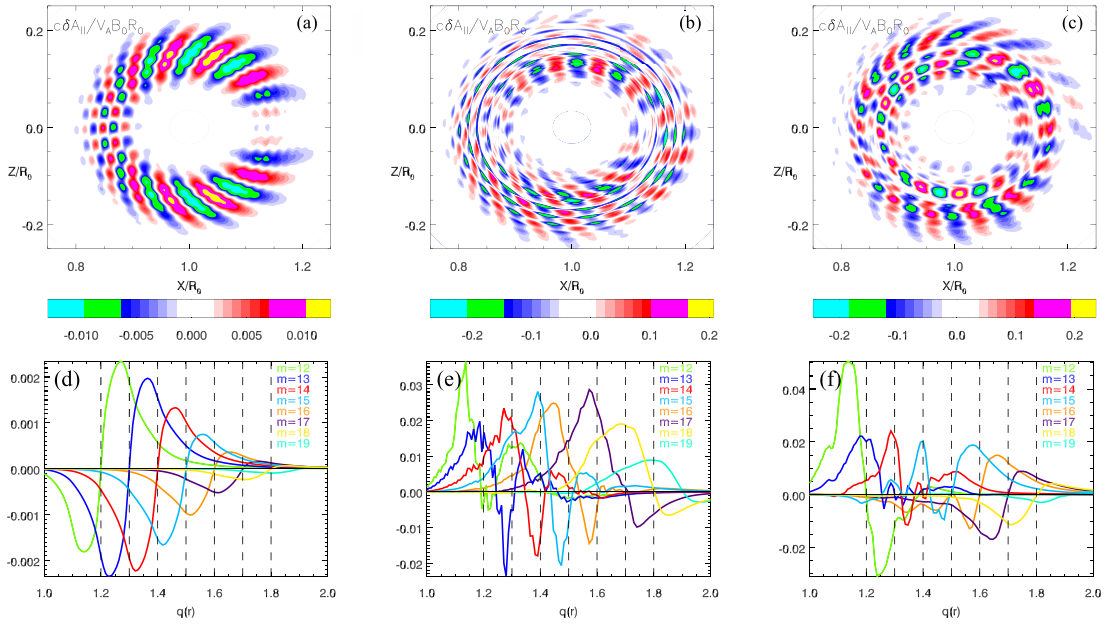

FIG. 4. Poloidal contour of the parallel vector potential $\delta A_{\parallel}$ linear structure before the intermediate regime in panel (a), and $\delta A_{\parallel}$ nonlinear structure after the intermediate regime in panel (b) in the simulation with self-consistent ponderomotive force. Panel (c) shows poloidal contour of nonlinear $\delta A_{\parallel}$ in the simulation without the ponderomotive force terms but with zonal flows. Panels (d), (e), and (f) show the radial profile of (n, m) harmonic of $\delta A_{\parallel}$ in (a), (b), and (c).

role of resistive tearing physics[29] in the saturation of KBM. With resistivity 100 times the Spitzer resistivity, no significant tearing instability is observed within the time scale of KBM nonlinear saturation. In this case, the KBM linear growth rate and real frequency are increased significantly by the resistive drive, and the zonal fields still saturate the mode with a radially smoother nonlinear mode structure.

Conclusions and future work.—In summary, we have presented global gyrokinetic simulation results of KBM nonlinear behavior. The instability develops into an intermediate regime, followed by nonlinear saturation regulated by spontaneously generated zonal fields. In the intermediate regime, rapid growth of the localized current sheet is observed. These qualitative features appear to be robust consequences of our work and have potentially important consequences for space and fusion plasmas. In the Earth's magnetotail, where there has been significant controversy regarding the relative importance of ballooning modes and magnetic reconnection in causing substorm onset, our studies suggest that nonlinear KBMs, which are self-regulated by zonal flows, can produce thin current sheets that can be unstable to secondary tearing instabilities, thus enabling both mechanisms to play important roles at various stages of time-evolution in causing substorm onset. This perspective is similar to that presented in a recent MHD study,[30] except that the mechanism driving ballooning modes in our simulations is inherently kinetic. The simulations do not seem to exhibit plasmoid instabilities[31,32] which might be suppressed or stabilized due to diamagnetic effects. On a longer time scale, the current sheet near the rational surfaces might induce collisionless tearing instabilities, which can provide seed islands for the neoclassical tearing mode or plasmoid instabilities.[33] For future work, we plan to explore the consequences of coupling nonlinear KBM instabilities with magnetic reconnection in Earth's dipole magnetic field for the magnetotail and in tokamak edge configuration.

This research was supported by U.S. DOE Grant Nos. DE-AC02-09CH11466 and DE-FG02-07ER54916 and (DOE) SciDAC ISEP Center and used resources of the Oak Ridge Leadership Computing Facility at the Oak Ridge National Laboratory (DOE Contract No. DE-AC05-00OR22725) and the National Energy Research Scientific Computing Center (DOE Contract No. DE-AC02-05CH11231).

REFERENCES

[1]D. Dobrott, D. B. Nelson, J. M. Greene, A. H. Glasser, M. S. Chance, and E. A. Frieman, Phys. Rev. Lett. **39**, 943 (1977).
[2]O. A. Hurricane, B. H. Fong, S. C. Cowley, F. V. Coroniti, C. F. Kennel, and R. Pellat, J. Geophys. Res. **104**, 10221, https://doi.org/10.1029/1999JA900012 (1999).
[3]P. Zhu, C. R. Sovinec, C. C. Hegna, A. Bhattacharjee, and K. Germaschewski, J. Geophys. Res. **112**, A06222, https://doi.org/10.1029/2006JA011991 (2007).
[4]A. Kirk, B. Koch, R. Scannell, H. R. Wilson, G. Counsell, J. Dowling, A. Herrmann, R. Martin, and M. Walsh (the MAST team), Phys. Rev. Lett. **96**, 185001 (2006).
[5]E. D. Fredrickson, K. M. McGuire, Z. Y. Chang, A. Janos, J. Manickam, and G. Taylor, Phys. Plasmas **3**, 2620 (1996).
[6]A. Diallo, R. Maingi, R. Maingi, S. Kubota, A. Sontag, T. Osborne, M. Podesta, R. E. Bell, B. P. LeBlanc, J. Menard, and S. Sabbagh, Nucl. Fusion **51**, 103031 (2011).
[7]H. R. Wilson and S. C. Cowley, Phys. Rev. Lett. **92**, 175006-1 (2004).
[8]S. C. Cowley and M. Artun, Phys. Rep. **283**, 185 (1997).
[9]P. Zhu, A. Bhattacharjee, and K. Germaschewski, Phys. Rev. Lett. **96**, 065001 (2006).
[10]P. Zhu, C. C. Hegna, C. R. Sovinec, A. Bhattacharjee, and K. Germaschewski, Nucl. Fusion **49**, 095009 (2009).
[11]P. B. Snyder, R. J. Groebner, A. W. Leonard, T. H. Osborne, and H. R. Wilson, Phys. Plasmas **16**, 056118 (2009).
[12]D. Dickinson, C. M. Roach, S. Saarelma, R. Scannell, A. Kirk, and H. R. Wilson, Phys. Rev. Lett. **108**, 135002 (2012).
[13]C. Z. Cheng and A. T. Y. Lui, Geophys. Res. Lett. **25**, 4091, https://doi.org/10.1029/1998GL900093 (1998).
[14]P. L. Pritchett and F. V. Coroniti, J. Geophys. Res. **115**, A06301, https://doi.org/10.1029/2009JA014752 (2010).
[15]M. J. Pueschel, M. Kammerer, and F. Jenko, Phys. Plasmas **15**, 102310 (2008).
[16]S. Maeyama, A. Ishizawa, T.-H. Watanabe, M. Nakata, N. Miyato, M. Yagi, and Y. Idomura, Phys. Plasmas **21**, 052301 (2014).
[17]A. Ishizawa, T.-H. Watanabe, H. Sugama, M. Nunami, K. Tanaka, S. Maeyama, and N. Nakajima, Nucl. Fusion **55**, 043024 (2015).
[18]R. E. Waltz, Phys. Plasmas **17**, 072501 (2010).
[19]C. H. Ma and X. Q. Xu, Nucl. Fusion **57**, 016002 (2017).
[20]Z. Lin, T. S. Hahm, W. W. Lee, W. M. Tang, and R. B. White, Science **281**, 1835 (1998).
[21]W. Deng, Z. Lin, and I. Holod, Nucl. Fusion **52**, 023005 (2012).
[22]I. Holod, W. L. Zhang, Y. Xiao, and Z. Lin, Phys. Plasmas **16**, 122307 (2009).
[23]G. Dong, J. Bao, A. Bhattacharjee, A. Brizard, Z. Lin, and P. Porazik, Phys. Plasmas **24**, 081205 (2017).
[24]J. Bao, D. Liu, and Z. Lin, Phys. Plasmas **24**, 102516 (2017).
[25]L. Chen and F. Zonca, Rev. Mod. Phys. **88**, 015008 (2016).
[26]T. S. Hahm, P. H. Diamond, O. D. Gurcan, and G. Rewoldt, Phys. Plasmas **14**, 072302 (2007).
[27]E. A. Belli and J. Candy, Phys. Plasmas **17**, 112314 (2010).
[28]L. Chen, Z. Lin, and R. White, Phys. Plasmas **7**, 3129 (2000).
[29]D. Liu, W. Zhang, J. McClenaghan, J. Wang, and Z. Lin, Phys. Plasmas **21**, 122520 (2014).
[30]P. Zhu, A. Bhattacharjee, A. Sangari, Z. Wang, and P. Bonofiglo, Phys. Plasmas **24**, 024503 (2017).
[31]A. Bhattacharjee, Y.-M. Huang, H. Yang, and B. Rogers, Phys. Plasmas **16**, 112102 (2009).
[32]S. Günter, Q. Yu, K. Lackner, A. Bhattacharjee, and Y.-M. Huang, Plasma Phys. Controlled Fusion **57**, 014017 (2015).
[33]F. Ebrahimi, Phys. Plasmas **24**, 056119 (2017).